ELSEVIER

Journal of Molecular Catalysis A: Chemical 181 (2002) 291–301

JOURNAL OF MOLECULAR CATALYSIS A: CHEMICAL

www.elsevier.com/locate/molcata

An attempt to predict the optimum zeolite-based catalyst for selective cracking of naphtha-range hydrocarbons to light olefins

B.G. Anderson [a], R.R. Schumacher [a,1], R. van Duren [a], A.P. Singh [a,b], R.A. van Santen [a,*]

[a] *Laboratory of Inorganic Chemistry and Catalysis, Schuit Institute of Catalysis, Eindhoven University of Technology, P.O. Box 513, 5600 MB Eindhoven, The Netherlands*

[b] *Catalysis Division, National Chemical Laboratory, Pune 411 008, India*

Received 23 January 2001; received in revised form 20 August 2001; accepted 27 August 2001

Abstract

Theoretical calculations were performed in order to determine, a priori, which in a range of small-to-medium pore zeolites would be the most effective at suppressing hydride transfer reactions by estimating the magnitude of steric hindrance. Steric hindrance was estimated as the difference between the enthalpies of adsorption of the transition-state complex and those of the two reacting hydrocarbons, calculated using the configurational-bias Monte Carlo (CBMC) method. As the concentration of adsorbed heptane also affects reaction rates adsorption equilibria were also calculated using this same theory.

Heptane cracking experiments were then performed using acidic catalysts of this same series of zeolites to test the validity of these predictions. Reaction products were sampled during the first seconds on stream and extrapolation was made to zero time on stream in order to determine the initial catalytic activities and product selectivities in the absence of deactivation.

Turnover frequency (TOF) decreased with decreasing pore diameter in agreement with predicted heptane adsorption equilibria. Hydride transfer was predicted to be most restricted in FER and TON, however, lower heptane adsorption capacities suggested that MFI would be the best compromise in terms of both high activity and selectivity.

Although differences in paraffin product differences were observed that were consistent with an increasing degree of protolytic cracking with decreasing pore size, no discernible pattern was observed in olefin product distributions (ethylene–butenes).

Keywords: Alkane cracking; Cracking on zeolites; Hydride transfer; Steric hindrance; Olefin production

1. Introduction

Acidic zeolite-catalysed cracking of alkanes has been the extensively studied. It is now generally accepted that cracking occurs via two different mechanisms [1–3]. Classical cracking takes place when branched secondary and tertiary alkylcarbenium ions derived from the feed molecule are cleaved by a single beta-scission into smaller alkylcarbenium ions and alkenes. Products formed during the catalytic cracking of a C_nH_{2n+2} alkane via this mechanism trend to possess carbon numbers within the range 3 to $n-3$. Hence, using *n*-heptane as an example, equal amounts of C_3 and C_4 hydrocarbons result. The formation of primary alkylcarbenium ions is unlikely and so ethylene, ethane and methane are

* Corresponding author. Tel.: +31-40-247-3082; fax: +31-40-245-5054.
E-mail address: r.a.v.santen@tue.nl (R.A. van Santen).
[1] Present address: Lufthansa Systems GmbH, D-60549 Frankfurt, Germany.

1381-1169/02/$ – see front matter
PII: S1381-1169(01)00374-0

not observed. Bimolecular hydride transfer reactions between alkylcarbenium ions and feed alkanes lead to chain reactions that produce shorter alkanes thus limiting the yield of olefins to 50%.

A second mechanism, proposed in 1984 by Haag and Dessau, is now also widely accepted. In this mechanism, called "protolytic cracking", alkanes are protonated to form carbonium ion transition states that can undergo either C–C bond cleavage yielding alkanes (including methane and ethane) or C–H bond cleavage yielding dihydrogen and carbenium ions. These carbenium ions subsequently form alkenes via back-donation of a proton to the zeolite [2]. The formation of ethylene is possible via this mechanism.

Experimentally, it has been observed that alkane cracking on small- and medium-pore zeolites (such as FER and MFI) occurs predominantly via the protolytic cracking mechanism [4]. This is generally believed to be due to steric limitations as smaller micropores hinder the formation of the hydride transfer transition state. This is an example of a so-called "shape-selectivity" effect. In addition, protolytic cracking is favoured under conditions where the concentration of alkenes is low since alkenes are better proton acceptors than alkanes.

The so-called "constraint index (CI) test" was proposed by Haag and co-workers [5] in an attempt to empirically quantify zeolite shape-selectivity effects on the rate of alkane cracking and is now widely used. The test is designed to compare the rates at which *n*-hexane and one of its isomers, 3-methylpentane, are cracked under similar conditions. In the absence of steric effects, the branched isomer cracks more quickly. Several other such empirical criteria quantifying the effects of shape-selectivity have since been proposed, see [6] for an interesting discussion.

Although empirical quantification of steric effects via the calculation of indices such as the CI mentioned above is without doubt very useful, it is desirable to try to develop theoretical (or at least semi-empirical) methods by which shape-selective effects can be quantitatively (or semi-quantitatively) calculated a priori. Such methods can then be used to predict the zeolite structures and experimental conditions that have the greatest chance of success. To date such predictive tools remain limited.

Quantum chemical methods have now been applied to study a great number of different elementary alkane conversion reactions that occur on acidic zeolite catalysts (see, e.g. [7] for a review of these calculations). Such calculations are capable of predicting the structures of transition-state complexes, the activation energies to their formation, etc. These calculations have, however, mainly been performed utilising relatively small silica–alumina clusters with isolated Bronsted acid sites as models. Such models have limited ability to take into account the interaction of the transition-state complex with the chemical environment, i.e. interactions with the pore walls of the zeolite. It is precisely this interaction that we need to quantify in order to predict the degree to which shape-selectivity effects will influence alkane cracking in different zeolite structures. Therefore, we must use methods in addition to quantum chemical cluster models. In this work, we have used the so-called configurational-bias Monte Carlo (CBMC) method [8].

We have tried to determine, a priori, which of a range of small- to medium-pore zeolites would be most effective at suppressing beta-cracking of a naphtha-range alkane (*n*-heptane) by estimating the magnitude of steric hindrance using theoretical calculations. Steric hindrance to the formation of the hydride transfer complex was estimated as the difference between the enthalpies of adsorption of the transition-state complex and those of the two reacting hydrocarbons, calculated using the CBMC method. As reaction rates are not only influenced by changes in activation energies but also are affected by changes in the concentration of adsorbed heptane adsorption equilibria were also calculated using this same theory.

Heptane cracking experiments were performed using acidic catalysts of this same series of zeolites to test the validity of the predictions. Reaction products were sampled during the first seconds on stream and extrapolation was made to zero time on stream in order to determine the initial catalytic activities and product selectivities in the absence of deactivation.

2. Theory

The transition states involved in hydride transfer reactions between an adsorbed alkoxy species and feed alkanes are believed to be bridged, bimolecular structures [7]. For example, the hydride transfer complex

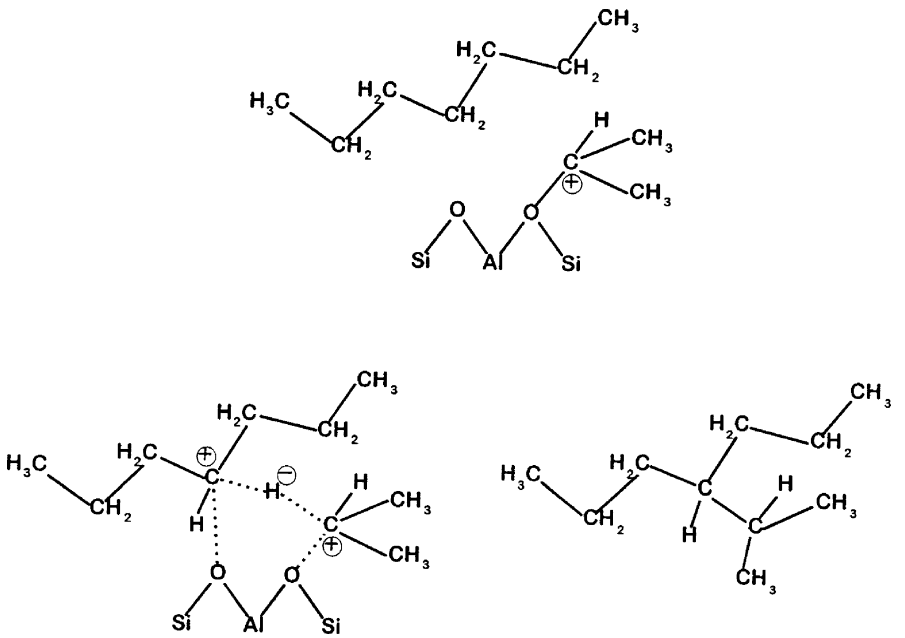

Fig. 1. Structure of (top) an adsorbed propoxy species and with feed molecule of *n*-heptane (lower left) transition-state complex for hydride ion transfer (lower right) branched hydrocarbon (e.g. 4-isopropylheptane) used to approximate complex in CBMC simulations.

formed between an adsorbed propoxy species and a solvent *n*-heptane molecule is shown in Fig. 1. One can approximate the structure of this complex using a branched hydrocarbon such as 4-isopropylheptane (also shown).

In this study, we have assumed that the transition-state complex for hydride transfer has the structure of a branched hydrocarbon as discussed above. The steric hindrance experienced between this "complex" and the zeolite micropore is assumed to be equal to difference between the heat of adsorption of the branched hydrocarbon molecule and the sum of the heats of adsorption of the two separate hydrocarbons that form it.

Thus the steric energy contribution to the activation energy can then be calculated according to the following equation.

$$E_{\text{steric}} = \Delta H_{\text{ads}}^{\text{TS model}} - \Delta H_{\text{ads}}^{\text{reactant 1}} - \Delta H_{\text{ads}}^{\text{reactant 2}} \quad (1)$$

Two extreme cases can be considered. Firstly, if there are no steric effects, the heat of adsorption of the model molecule simulating the transition state should be identical to the sum of the heats of adsorption of its two constituent molecules. (It is assumed that the energy contribution of the alkoxy-group due to the physical interaction with the pore walls is identical to the heat of adsorption of the respective alkane.) The other extreme case occurs when the transition state is too large to be incorporated into the zeolite framework. In this case, E_{steric} calculated in Eq. (1) would be infinite.

2.1. The simulation method

Calculations were performed making use of Grand Canonical Monte Carlo simulations to represent the adsorbed alkanes in the zeolite structures. The so-called configurational-bias algorithm of Smit and Siepmann [9,10] was used in order to simulate these larger adsorbate molecules. The reader is referred to these publications for further information regarding the theory. The latest version of their program was used [11].

The zeolite lattice structure was assumed to be purely siliceous and static. Neither lattice defects nor charge compensating cations were taken into account. A united-atom van der Waals type potential was employed for the interactions between adsorbate

Table 1
Potential parameters of the so-called nature-potential used in CBMC simulations

Interaction	ε (K)	σ (Å)
CH_3–O	87.5	3.64
CH_2–O	54.4	3.64

molecules and zeolite. These interaction parameters are listed in Table 1.

Several of the zeolite structures frequently used in catalysis research were included in the simulations. Their most important properties are summarised in Table 2.

The zeolite structures MFI, MOR and BEA were chosen as these are amongst the most commonly used as zeolite catalysts. FER and TON seemed to be promising candidates as their pore diameters are smaller than those above and thus larger steric effects were more likely. Although MFI has approximately the same pore diameters as found in FER and TON, large intersections are present between the two channels in this structure that can accommodate larger sorbates. Practically speaking, the one-dimensional channel system of TON and the quasi-one-dimensional system of FER may have disadvantages in connection with deactivation processes. CHA was chosen as its AlPO4-analogue, SAPO-34, was regarded an interesting candidate for this reaction. ERI offered a potential alternative 8-ring zeolite. The faujasite structure (FAU) was not included in this study since shape selective properties were not expected in this relatively large pore zeolite.

Normal heptane was chosen as the main feed gas as it is a major component of naphtha-range hydrocarbons. Due to the large number of combinations of reactants possibly undergoing hydride transfer reactions, a choice of representative reactants and transition states had to be made. As C_3- and C_4-hydrocarbons represent the largest fraction of the cracking products transition states for C_3–C_3, C_3–C_4, C_4–C_4 and C_3–C_7 were selected. It should be emphasised that within the model which of the two reactants is present as the alkoxy-group or as the alkane does not play a role as the physical interaction of both is calculated from the interaction of the respective alkane.

3. Experimental

Cracking experiments were performed using *n*-heptane over various acidic zeolites in order to test the theoretical predictions. Four different zeolites were examined: ZSM-22, FER, ZSM-5, and MOR. All zeolites were obtained from Shell Research and Technology Centre Amsterdam, The Netherlands. Table 3 contains information concerning the properties of the zeolites used.

Normal heptane (Merck, purity > 99%) was used as received. Helium (99.99%) was used as a carrier gas. Experiments were performed in a single-pass, plug-flow microreactor system. Gas flows were controlled using Brooks mass-flow controllers. Heptane flow was controlled using a Hewlett-Packard 1050 HPLC pump. The alkane was vaporised at 100 °C into the helium carrier gas.

A quartz glass tube micro-reactor (internal diameter 4 mm) typically containing 70 mg of catalyst particles (125–425 μm diameter) was used. Samples were collected on-line using a 16-loop sample valve (Valvo

Table 2
Relevant data for zeolite structures investigated by CBMC[a]

Structure type	Dimensionality	Pore diameter (Å)	Crystallography density (g/cm^3)	Structure of pore system
BEA	3 (12-ring)	5.5 × 5.5, 7.6 × 6.4	1.51	Channel
MOR	1 (12-ring)	6.5 × 7.0	1.72	Channel
MFI	3 (10-ring)	5.3 × 5.6, 5.1 × 5.5	1.743	Channel
TON	1 (10-ring)	4.4 × 5.5	1.99	Channel
FER	1 (10-ring) (2/8-ring)	4.2 × 5.4 (3.5 × 4.8)	1.77	Channel
CHA	3 (8-ring)	3.8 × 3.8	1.38	Cage
ERI	3 (8-ring)	3.6 × 5.1	1.59	Cage

[a] Crystallographic density was calculated for a purely siliceous structure.

Table 3
Physical, chemical and structural properties of zeolites used in heptane cracking experiments

Property	Ferrierite	Mordenite	ZSM-5	ZSM-22
Structural group	FER	MOR	MFI	TON
Chemical formula	$Na_n[Al_nSi_{36-n}O_{72}]\cdot 18H_2O$	$Na_n[Al_nSi_{48-n}O_{96}]\cdot 24H_2O$	$Na_n[Al_nSi_{96-n}O_{192}]\cdot \sim 16H_2O$	$Na_n[Al_nSi_{24-n}O_{48}]\cdot \sim 4H_2O$
Si/Al (mol mol^{-1})	10.3	5	41.6	44.7
n	3.19	8	2.25	0.525
M_w (g mol^{-1})	2486.7	3315.5	6120.1	1514.0
[H$^+$] (mol g^{-1})	1.21×10^{-3}	2.41×10^{-3}	3.68×10^{-4}	3.47×10^{-4}
# Channels	2	2	2	1
Direction, 1	[0 0 1]	[0 0 1]	[0 1 0]	[0 0 1]
# O-atoms, 1	10	12	10	10
Free diameter, 1 (Å)	4.2×5.4	6.5×7.0	5.3×5.6	4.4×5.5
Dimension, 1	1	1	3	1
Direction, 2	[0 1 0]	[0 1 0]	[1 0 0]	–
# O-atoms, 2	8	8	10	–
Free diameter, 2 (Å)	3.5×4.8	2.6×5.7	5.1×5.5	–
Dimension, 2	1	1	3	–
Interconnected	Yes	Yes	Yes	–

Instruments). The products were analysed on a gas chromatograph (Shimadzu, GC-17A) with a fused silica column (PLOT fused silica, 50 m × 0.53 mm inside, Al_2O_3/KCl 10 μm film) and an FID detector.

The reactor was heated to 120 °C at a rate of 5 °C min^{-1} and kept at this temperature for 1 h in order to remove most of the (physisorbed) water. Afterwards, the reactor was heated to the desired temperature, typically 550 °C. The reactor was equilibrated at this temperature for 1 h prior to an experiment.

Single-pass flow experiments were performed at atmospheric pressure. The *n*-heptane/helium ratio was typically 1:19 (v/v). In order to minimise the effects of deactivation, the activity was measured at very short times on stream. Initial activity of the catalysts was measured by collecting 15 samples, one every 5 s, beginning after a predetermined deadtime necessary for the sample to reach the storage loop. The first sample was defined as that in which the total integrated area of all measured peaks became constant. This ensured that complete filling of the sample loops was obtained and that the measurements were free from pressure effects due to the initial valve switching necessary to start the experiment. Carbon mass balances were checked by comparing the total amounts of carbon-containing species as measured by GC with the amounts of reactant *n*-heptane flowed through a reactor bed of silica under the same conditions.

The measured *n*-heptane conversion, X, was plotted versus time on stream for the first minute of reaction. Numerical extrapolation was used to obtain the initial conversion (at time $t = 0$ s) in order to eliminate the effects of deactivation as previously reported [13,14].

The apparent rate constant for reaction (k_0) was calculated using the relation:

$$k_0 = -\mathrm{WHSV}\ln(1 - X)$$

Turnover frequencies (TOF) for *n*-heptane reaction were calculated via

$$\mathrm{TOF} = \frac{k_0}{N_H M_r}$$

where N_H is the number of theoretical maximum number of Bronsted acid sites available in the zeolite, based on its Si/Al ratio.

4. Results

Fig. 2 shows the predicted steric energies calculated according to Eq. (1) for the four transition states chosen, in the different zeolite frameworks. From these results, the zeolite structures can roughly be subdivided into three categories according to the degree of predicted steric hindrance. Firstly, almost no steric energy contribution was predicted in the case of the BEA,

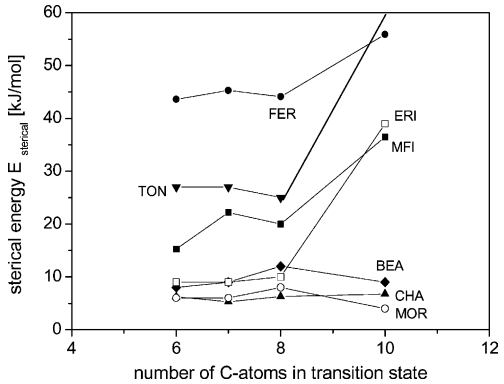

Fig. 2. Steric energy (calculated according to Eq. (1)) for hydride transfer transition-state complexes between hydrocarbons of various lengths (from C_3–C_3 to C_3–C_7) in zeolite structures of different pore size and structure.

MOR, CHA and ERI structures. Secondly, the TON and MFI-structures represent an intermediate degree of steric constraint with one very notable exception; this being the case of the C_{10} transition state, modelled by 4-isopropylheptane, in TON. No adsorption sites could be found for this molecule. It could not be inserted into the zeolite micropore. Hence the steric contribution predicted was infinite. Thus, hydride transfer between C_3 and *n*-heptane was predicted to be impossible within the TON structure. Thirdly, severe steric hindrance to hydride transfer was predicted for the FER structure. All transition states tested had a steric contribution of between 45 and 55 kJ/mol.

It can be seen in Fig. 2 that the calculated steric energy for the largest transition state used (C_{10}) was significantly higher than that of the others in FER, TON, ERI, and MFI and was most extreme in the case of TON as discussed above. Hence hydride transfer between C_3 and *n*-heptane is predicted to be sterically more hindered in these structures than transfer between smaller hydrocarbons.

The estimated accuracy of the numerical results is about ±3–4 kJ/mol. Although the calculated steric interactions in the cases of BEA, MOR, CHA and ERI are small, they are nonetheless greater than the estimated error margin and must, therefore, be regarded as real. The general uncertainty of the calculated data is difficult to estimate because various assumptions have to be made within the model. As the parameter-set for the forcefield used for the current simulation were developed for systems in which the contact between sorbate and zeolite is less intense, it is not totally clear if the repulsive part of the Lennard–Jones-potential is modelled accurately enough for a precise quantitative prediction of the steric energy. Whether or not the united-atom-approach gives a sufficiently exact approximation of the physical reality under these extreme conditions is also unclear. Furthermore, electrostatic interactions due to polarisation effects possibly influencing the activation energy have not been taken into account. The present results should, therefore, be considered to be semi-quantitative predictions.

4.1. Adsorption of heptane

Fig. 3 shows the equilibrium adsorption constant for *n*-heptane (calculated at $T = 675$ K), as a qualitative measure for the physical adsorption, as a function of pore size (decreases from left to right). As shown, the equilibrium adsorption constant decreases with increasing pore diameter for zeolites MOR through TON.

Table 4 lists the equilibrium adsorption constants calculated for propane, *n*-butane and *n*-heptane in FER, MOR, ZSM-5 and ZSM-22 at 675 and 775 K.

Fig. 4 shows the measured *n*-heptane conversion (mol%) as a function of time on stream for

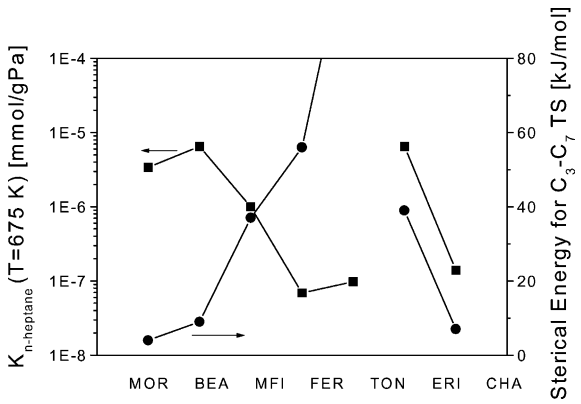

Fig. 3. Equilibrium adsorption constant for *n*-heptane (at 675 K) calculated using CBMC calculations plotted as a function of zeolite structure (squares). The pore diameter of the zeolite essentially decreases from left to right. The steric energy (calculated according to Eq. (1)) for hydride transfer transition-state complexes between C_3 and C_7 hydrocarbons in these zeolites is also plotted (right-hand axis, circles).

Table 4
Equilibrium adsorption constants for propane, *n*-butane and *n*-heptane on various zeolite types at different temperatures

	K ($T = 675$ K) (mmol g^{-1} Pa^{-1})	K ($T = 775$ K) (mmol g^{-1} Pa^{-1})	ΔH_{ads} (kJ mol^{-1})
Ferrierite			
n-Heptane	6.9×10^{-8}	1.0×10^{-8}	−84
n-Butane	5.2×10^{-8}	1.79×10^{-8}	−47
Propane	1.29×10^{-7}	4.9×10^{-8}	−42
Mordenite			
n-Heptane	3.4×10^{-6}	5.3×10^{-7}	−78
n-Butane	6.3×10^{-7}	2.3×10^{-7}	−44
Propane	4.0×10^{-7}	1.65×10^{-7}	−38
ZSM-5			
n-Heptane	1.0×10^{-6}	1.53×10^{-7}	−82
n-Butane	5.7×10^{-7}	1.81×10^{-7}	−50
Propane	3.7×10^{-7}	1.49×10^{-7}	−40
ZSM-22			
n-Heptane	9.6×10^{-8}	1.31×10^{-8}	−87
n-Butane	1.25×10^{-7}	3.6×10^{-8}	−54
Propane	8.1×10^{-8}	3.0×10^{-8}	−43

various acidic zeolite catalysts at 550 °C (He/nC$_7$ = 19, 15 h^{-1}). Marked deactivation was measured for all catalysts. As can be seen, all four catalysts lost considerable activity within the first 300 s on stream. FER was totally deactivated after 5 min on stream. TON and MFI lost circa 50% of their initial activities during this period; MOR lost circa 66%.

Fig. 5 shows the activity of the catalysts expressed in terms of heptane TOF. These data were measured at 550 °C at *n*-heptane conversions between 20 and 40%. The zeolites are ordered such that the pore diameter decreases from top to bottom. Thus the TOF measured on these acidic zeolites decreased monotonically with decreasing pore size from HMOR to HFER, i.e. the measured order of activity was: HMOR ≫ HZSM-5 > HZSM-22 > HFER.

The initial product distributions included: alkanes from methane to pentanes, ethylene, propylene, butenes and hydrogen. No aromatics (benzene, toluene or xylenes) were measured at heptane conversions below 50%. Initial carbon balances ($t = 0$) were 100% within experimental error. Thus the effects of deactivation due to coking can be corrected by this extrapolation method.

As the production of light olefins was of primary interest in this work, the selectivity to olefins (ethylene–butenes) was as important as the reaction rates. Olefin selectivities measured at 550 °C (He/nC$_7$ = 19) on each of the four acidic zeolites at conversion levels between 20 and 40% are compiled in Table 6. As shown, the total olefin selectivity was virtually independent of zeolite structure and equalled 65–70%. The relative selectivities to the three olefins, relative to both propylene and to ethylene, are also shown in the table.

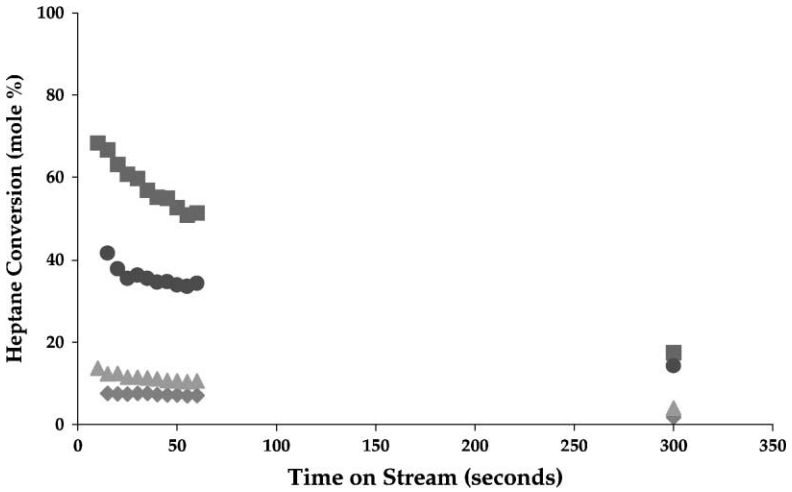

Fig. 4. Heptane conversion (mol%) versus time on stream (s) measured at 5 s intervals during the first few minutes on-line is plotted for several different acidic zeolites: HMOR (squares); HZSM-5 (circles); HZSM-22 (triangles) and HFER (diamonds). Experimental conditions: 5 vol.% *n*-heptane in helium, 550 °C, 70 mg zeolite, WHSV = 15 h^{-1}.

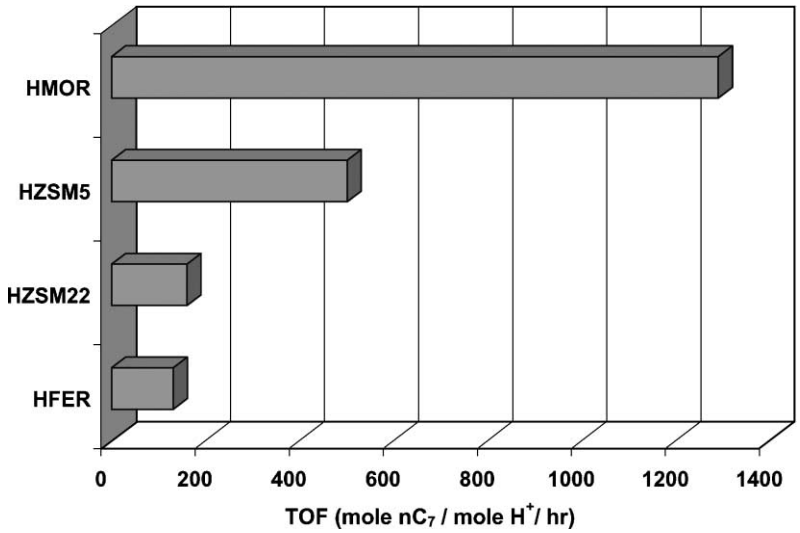

Fig. 5. Measured initial TOF (in mol *n*-C_7/mol H^+/h), calculated via extrapolation to zero time-on-stream, plotted versus acidic zeolite type. Experimental conditions as given in Fig. 4. Heptane conversion level between 30 and 40 mol%. Pore diameter of zeolite essentially decreases from top to bottom.

Fig. 6 shows the paraffin product distributions for the above experiments. Methane was detected in the products in each case, however, no hexanes were found. The amount of pentane measured in each experiment was always less than that of ethane. It is of interest to note that the amount of isobutane formed (via beta-scission of C_7) decreased with decreasing zeolite pore diameter. Less ethane, *n*-butane and *n*-pentane were formed on HMOR than on the smaller-pore zeolites. However, the amount of propane formed was similar and indeed the most methane was produced on HMOR.

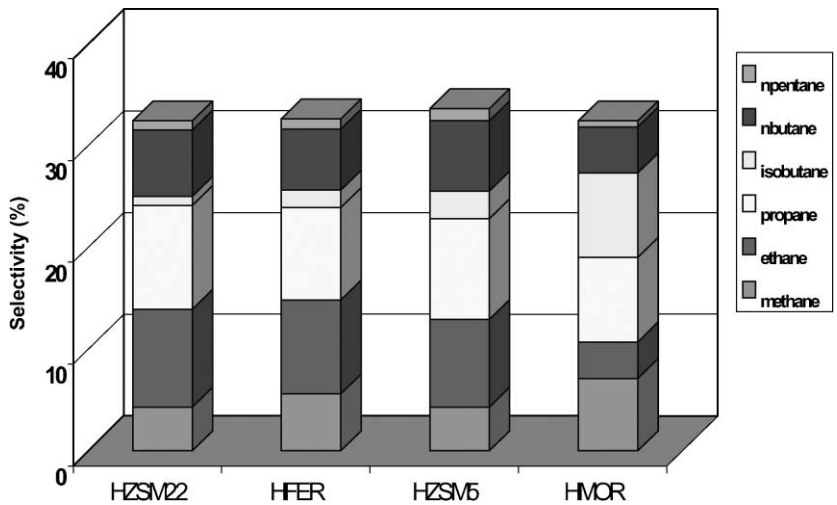

Fig. 6. Initial selectivities (mol%) to paraffinic products measured at 30% *n*-heptane conversion level plotted against zeolite type. Pore diameter of zeolite essentially increases from left to right. Experimental conditions as given in Fig. 4.

5. Discussion

It is known from earlier simulations that the pore geometry not only influences the energy of the transition state but also exerts some influence on the physical adsorption properties of hydrocarbons in the various zeolite types [9,10]. Adsorption constants can generally related to the heat and the entropy of adsorption by the following equation:

$$RT \ln K_{ads} = T\Delta S_{ads} - \Delta H_{ads} \quad (2)$$

It is also known that the heat and entropy of adsorption of hydrocarbons in many zeolitic systems are related by what is frequently referred to as a compensation effect, given in the following equation [12]:

$$\Delta S_{ads} \propto \Delta H_{ads} \quad (3)$$

Eq. (3) can be understood by the fact that a sorbate molecule that is tightly bound to the zeolite (i.e. possesses a large heat of adsorption) is also more localised at a defined adsorption site and is, therefore, less mobile (i.e. experiences a large entropy loss upon adsorption). For adsorption of a hydrocarbon in a zeolite with narrow pores, the adsorption constant is larger at low temperatures, but due to the larger heat of adsorption, it decreases faster at increasing temperatures. Due to the compensation effect, the entropy loss due to adsorption is also larger for the narrow pore zeolite. As a result, the adsorption constant of hydrocarbons in narrow pore zeolites becomes even lower than that in the large pore zeolite at elevated temperatures.

It is now interesting to correlate these two effects of the pore diameter for the different zeolite structures. Fig. 3 shows the equilibrium adsorption constant for *n*-heptane (calculated at $T = 675\,K$), as a qualitative measure for the physical adsorption, as a function of pore size (decreases from left to right). Fig. 3 also shows the calculated steric energy for the largest transition state (C_{10}) as a measure for the steric influence on the reaction rate.

A correlation is difficult to find in Fig. 3 for the cage-type structures CHA and ERI, but for the channel-type structures, it is obvious that while the adsorption constant in essence decreases with decreasing pore diameter (BEA, MOR, MFI, FER, TON) the steric energy increases. This has considerable consequences for the selective cracking of *n*-heptane towards small olefins over zeolite-based catalysts. One of the prerequisites of a high conversion is a reasonably favourable physical adsorption, otherwise the concentration of reactant molecules is too small. According to the simulations, however, this can—at least at reaction temperatures—only be achieved when the pore diameter is large enough and the small pore zeolites are unfavourable. As stated above, a small pore diameter is desired for the suppression of hydride transfer in order to increase the selectivity to olefins. If the *yield* of olefins is to be optimised, a compromise concerning the pore diameter of the zeolite structure has to be found as it is impossible to optimise the pore diameter for both conversion and selectivity.

The results of the simulations are basically in agreement with the expectation that zeolites with 12-ring pores (BEA, MOR) or with cage structure (CHA, ERI) exert a smaller steric influence on the adsorbed molecules/transition states than do zeolites with 10-ring pores (MFI, TON, FER). The fact that CHA and ERI are especially able to accommodate bulky structures in spite of their 8-ring openings might be surprising at first sight. However, it has to be taken into account that the cages of those structures are significantly larger than the 8-ring openings suggest and thus larger molecules can be located there even if they are not able to diffuse out of the zeolite. This effect might, however, lead to rapid deactivation and thus other problems are created.

It is interesting to examine the amount of influence that steric contributions of the magnitude calculated (between circa 10 and 60 kJ/mol) would exert on the reaction rate due to the increase in the activation energy. Table 5, therefore, gives the extent to which the original reaction rate, r_0, would be reduced at various temperatures. As shown, a small contribution (10 kJ/mol) would lead to an 80% reduction in rate at 725 K (500 °C). A large contribution (60 kJ/mol) would slow the rate by more than 50,000 times.

As shown in Fig. 5, the initial heptane TOF decreased in the order HMOR > HZSM-5 > HZSM-22 > HFER. As mentioned previously, this is also the order of decreasing pore diameter. Fig. 3 shows that this is also the order of decreasing calculated heptane adsorption capacity. Previous studies of the pore dependence of the rate of *n*-heptane on HFER, HZSM-5, HMOR and HY found a maximum activity for HZSM-5, i.e. HZSM-5 > HFER ≈ HMOR > HY [13]. As the experimental conditions were not

Table 5
Reduction in reaction rate calculated at different reaction temperatures for different steric energy contributions

E_{steric} (kJ/mol)	r/r_0 ($T = 298$ K)	r/r_0 ($T = 675$ K)	r/r_0 ($T = 723$ K)	r/r_0 ($T = 775$ K)
10	0.018	0.17	0.19	0.21
20	3.1×10^{-4}	0.028	0.036	0.045
30	5.5×10^{-6}	0.0048	0.0068	0.0095
40	9.7×10^{-8}	8.0×10^{-4}	0.0013	0.0020
50	1.7×10^{-9}	1.4×10^{-4}	2.4×10^{-4}	4.3×10^{-4}
60	3.0×10^{-11}	2.3×10^{-5}	4.6×10^{-5}	9.0×10^{-5}
70	5.4×10^{-13}	3.8×10^{-6}	8.7×10^{-6}	1.9×10^{-5}

identical (450 °C, 5 atm, He/nC$_7$ = 4 mol/mol), it is uncertain if these results are directly comparable.

The measured selectivity to olefins (C$_2$–C$_4$) (Table 6) was virtually independent of structure for the H-zeolites at conversions between 20 and 40% equally 65–70%. Selectivity greater than 50% (balance paraffins) indicates that heptane cracking occurs on all four of these zeolites to some extent by protolytic cracking in addition to beta-scission [14]. This is in agreement with previous results that protolytic cracking is favoured on small- to medium-pore zeolites as discussed in Section 1. However, although beta-cracking is supressed relative to protolytic cracking, it still occurs to some extent on each of the four zeolites as revealed by the presence of isobutane.

Although the total initial selectivity to paraffins was independent of which proton zeolite was used, the alkane product distributions (shown in Fig. 6) reveal, however, an interesting dependence on zeolite pore size at low conversion ($X = 30\%$). The decrease in the amount of isobutane produced as the zeolite pore size decreases is indicative of a decrease in the extent to which cracking via beta-scission occurs. This agrees with the principle premise and with the predictions discussed above. The lower amounts of ethane, *n*-butane and *n*-pentane formed on HMOR also indicate that protolytic cracking is less active on this zeolite than on the other smaller pore zeolites. Propane can be formed by either beta-scission or protolytic cracking, so its amount does not differ greatly on the four different zeolites. Methane, but no hexanes, was observed. Also the amounts of pentanes formed were always smaller than those of ethane. Thus C$_6$ and C$_5$ hydrocarbons must undergo secondary cracking on H-zeolites. It would appear that secondary cracking occurs to the greatest extent on HMOR, since it produced the highest yield of methane, but the lowest yield of pentanes. We note here that methane cannot be formed by beta-scission.

Table 6
Olefin selectivity (C$_2$–C$_4$) measured on various acidic zeolite catalysts (mol%), 550 °C, nC$_7$/He = 1/19, $X = 30\%$

Olefin	HZSM-22	HFER	HZSM-5	HMOR
Ethylene	10	17	13	10
Propylene	33	43	43	47
Butenes	23	7	13	13
Total	65	67	66	68
C$_4$/C$_2$	2.6	1.5	1.8	2.2
C$_3$/C$_2$	3.7	2.7	3.2	4.3
C$_4$/C$_3$	0.7	0.5	0.6	0.5
C$_2$/C$_3$	0.4	0.6	0.5	0.4

The absence of aromatics at these heptane conversion levels (30%), dilutions and temperature is consistent with previously published results by Watson et al. [15]. These authors found that no aromatics were produced during *n*-heptane cracking over H-ZSM-5 under similar conditions at conversions of less than 50%.

Unlike the paraffin distribution, no trend could be found in the olefin product distribution (ethylene–butenes). In all cases, propylene was formed in the largest amount. This product can be formed by both protolytic and by classical cracking. The fact that no trend existed for ethylene and butenes, which can only be formed by protolytic cracking, could be due to the occurrence of secondary reactions.

6. Conclusions

CBMC-based calculations predicted severe restrictions to hydride transfer for FER-type catalysts, while the MFI- and TON-structures formed intermediate

cases. Hardly any influence of the pore structure was predicted for catalysts of the BEA-, MOR-, CHA- and ERI-structural types. Although small pore diameters are predicted to produce the highest selectivity, larger pores were shown to adsorb more hydrocarbons at these temperatures. Thus in order to optimise yields of short olefins, a suitable compromise should be found. MFI was predicted to be the best.

Experimental results showed that the initial heptane TOF decreased in the order HMOR > HZSM-5 > HZSM-22 > HFER. As mentioned previously, this is also the order of decreasing pore diameter and also the order of decreasing calculated heptane adsorption capacity.

Since greater than 50 mol% olefins (balance paraffins) were formed, heptane cracking occurred on all four of these zeolites to some extent by protolytic cracking in addition to beta-scission. Significant differences in the selectivity to olefins (C_2–C_4) were not observed as between 65 and 70 mol% olefins were formed on all zeolites. Olefin product distributions followed no particular trend, possibly due to the occurrence of secondary reactions. Propylene, which can be formed by both primary and secondary cracking, was always the most abundant.

Some differences in the paraffin product distributions, particularly for ethane and isobutane, were observed that revealed changes in mechanisms on different zeolites. In general, the trends were consistent with the trend of decreasing cracking via beta-scission and increasing protolytic cracking as pore size decreased.

References

[1] A. Corma, A.V. Orchilles, Micropor. Mesopor. Mater. 35–36 (2000) 21.
[2] S. Kotrel, H. Knoezinger, B.C. Gates, Micropor. Mesopor. Mater. 35–36 (2000) 21.
[3] B.W. Wojciechowski, Catal. Rev.-Sci. Eng. 40 (3) (1998) 209.
[4] C. Mirodatos, D. Bartomeuf, J. Catal. 114 (1989) 121.
[5] V.J. Frillette, W.O. Haag, R.M. Lago, J. Catal. 67 (1991) 218.
[6] S.I. Jones, T.V. Harris, Micropor. Mesopor. Mater. 35–36 (2000) 31.
[7] A.M. Rigby, G.J. Kramer, R.A. van Santen, J. Catal. 170 (1997) 1.
[8] B. Smit, J.I. Siepmann, Science 264 (1994) 1118.
[9] B. Smit, J.I. Siepmann, J. Phys. Chem. 98 (1994) 8442.
[10] B. Smit, Mol. Phys. 85 (1995) 153.
[11] T. Vlugt, Bigmac Release 1.20, University of Amsterdam, Amsterdam, July 1998.
[12] F. Eder, J. Lercher, Zeolites 18 (1997) 75.
[13] A.F. Wielers, M. Vaarkamp, M.F.M. Post, J. Catal. 127 (1991) 51.
[14] A. Corma, P.J. Miguel, A.V. Orchilles, Appl. Catal. A 138 (1996) 57.
[15] B.A. Watson, M.T. Klein, R.H. Harding, Ind. Eng. Chem. Res. 35 (1996) 1506.